THE JOURNAL OF PHYSICAL CHEMISTRY B

Article

A Molecular Dynamics Study of Alkaline Earth Metal#Chloride Complexation in Aqueous Solution

James P. Larentzos, and Louise J. Criscenti

J. Phys. Chem. B, **2008**, 112 (45), 14243-14250 • DOI: 10.1021/jp802771w • Publication Date (Web): 23 October 2008

A Molecular Dynamics Study of Alkaline Earth Metal−Chloride Complexation in Aqueous Solution

James P. Larentzos and Louise J. Criscenti*

Geochemistry Department, Sandia National Laboratories, Albuquerque, New Mexico 87185

Received: March 31, 2008; Revised Manuscript Received: July 31, 2008

The relative stability of alkaline earth metals ($M^{2+} = Mg^{2+}$, Ca^{2+}, Sr^{2+}, and Ba^{2+}) and their chloride complexes in aqueous solution is examined through molecular dynamics simulations using a flexible SPC water model with an internally consistent set of metal ion force field parameters. For each metal−chloride ion pair in aqueous solution, the free energy profile was calculated via potential of mean force simulations. The simulations provide detailed thermodynamic information regarding the relative stability of the different types of metal−chloride pairs. The free energy profiles indicate that the preference for contact ion pair formation increases with ionic radius and is closely related to the metal hydration free energies. The water residence times within the first hydration shells are in agreement with residence times reported in other computational studies. Calculated association constants suggest an increase in metal−chloride complexation with increasing cation radii that is inconsistent with experimentally observed trends. Possible explanations for this discrepancy are discussed.

1. Introduction

Molecular dynamics simulations have been used extensively to study hydration shell behavior and ion pair association for NaCl solutions as a function of concentration and temperature.[1−12] Simulations have also been performed to study the solvation behavior of alkaline earth metals in aqueous solution as a function of concentration.[13−17] Modeling calculations for alkaline earth metal−chloride solutions have been compared to data from diffraction experiments,[13] and extended X-ray absorbance florescence spectroscopy (EXAFS).[16,18−20] The force field parameter sets developed for aqueous ions are usually validated on the basis of their ability to reproduce measured or ab initio calculated water−molecule coordination numbers, hydration shell structures, and hydration energies. Ion−ion interactions are assumed to be successfully predicted by the force field if all of the ion−water interactions are adequately described. To our knowledge, Chialvo et al.[1] is the only study that attempts to match observed bulk thermodynamic behavior to molecular simulation results. For the ion pair Na^+Cl^-, Chialvo et al.[1] studied the anion−cation potential of mean force using three different ion−water models, determined association constants for the ion pair, and compared these constants with those based on high temperature conductance experiments.

In this study, aqueous-phase molecular dynamics simulations are used to investigate alkaline earth metal−chloride ($MgCl^+$, $CaCl^+$, $SrCl^+$, and $BaCl^+$) speciation. Previous simulations on aqueous $CaCl_2$[13] and $SrCl_2$[16] solutions to examine ion solvation and pairing have been compared successfully to experimental diffraction and EXAFS data. Potential-of-mean-force calculations for the ion pairs $MgCl^+$,[21] $CaCl^+$,[15,22,23] and $SrCl^+$,[14] have all been reported. However, in our research, we are interested in determining if observed trends in alkaline earth metal−chloride speciation can be reproduced using molecular simulations. Therefore, we calculated the $M^{2+}-Cl^-$ potential of mean force profiles for $M^{2+} = Mg^{2+}$, Ca^{2+}, Sr^{2+}, and Ba^{2+} using a consistently derived force-field parametrization. The computed structural, energetic, and thermodynamic properties are compared with experimental and spectroscopic measurements below.

TABLE 1: Force Field Parameters for Aqueous Ions and SPC Water

ion	σ_{ii}(Å)	ε_{ii} (kcal/mol)	charge
Mg^{2+}	1.3976	0.8750	2.00
Ca^{2+}	2.3609	0.4497	2.00
Sr^{2+}	3.1024	0.1182	2.00
Ba^{2+}	3.7862	0.0471	2.00
Cl^-	4.4000	0.1001	−1.00
O (SPC)	3.1655	0.1554	−0.82
H (SPC)	0.0000	0.0000	0.41

2. Computational Models and Methods

Molecular dynamics simulations and potential-of-mean-force calculations were conducted to investigate alkaline earth metal−chloride speciation in aqueous solution. All simulations were performed with the LAMMPS software package.[24,25] The interatomic interactions between water and the ions are pairwise additive, where the short-ranged repulsion−dispersion interactions are described through a conventional 12-6 Lennard-Jones potential and the long-ranged electrostatic interactions are modeled with a Coulombic potential. The pairwise interaction energy between atoms i and j is given by the expression

$$U_{ij} = 4\varepsilon_{ij}\left(\left[\frac{\sigma_{ij}}{r_{ij}}\right]^{12} - \left[\frac{\sigma_{ij}}{r_{ij}}\right]^{6}\right) + \frac{q_i q_j e^2}{4\pi\varepsilon_0 r_{ij}} \quad (1)$$

where r_{ij} is the separation distance between two ions, σ_{ij} and ε_{ij} are the respective Lennard-Jones size and energy parameters, q_i is the charge on atom i, e is the elementary charge of an electron, and ε_0 is the permittivity of a vacuum. Water is represented by the simple point charge (SPC) water model[26] and combined with harmonic bond stretching (bond spring constant = 554.1349 kcal·mol^{-1}, equilibrium bond length = 1.0 Å) and angle bending terms (angle spring constant = 45.753 kcal·mol^{-1}, equilibrium

* To whom correspondence should be addressed. E-mail: ljcrisc@sandia.gov.

10.1021/jp802771w CCC: $40.75
Published on Web 10/23/2008

TABLE 2: The Average Simulation Cell Lengths and Average Concentrations for Each MCl_2 NPT Simulation[a]

	cell length (Å)	concentration (M)
Number of $MgCl_2$		
4	31.32	0.22
8	31.38	0.43
16	31.52	0.85
32	31.82	1.65
64	32.48	3.10
Number of $CaCl_2$		
4	31.32	0.22
8	31.38	0.43
16	31.53	0.85
32	31.84	1.65
64	32.60	3.07
Number of $SrCl_2$		
4	31.34	0.22
8	31.42	0.43
16	31.59	0.84
32	31.96	1.63
64	32.79	3.01
Number of $BaCl_2$		
4	31.35	0.22
8	31.44	0.43
16	31.65	0.84
32	32.09	1.61
64	33.06	2.94

[a] The cell length standard deviations are between 0.02 and 0.03 Å.

angle = 109.47°) from Teleman et al.[27] The alkaline earth metal (Mg^{2+}, Ca^{2+}, Sr^{2+}, Ba^{2+}) ion−water interaction parameters are taken from a previous study[28] which matched the measured hydration free energies of each ion with the rigid SPC water model. The chloride ion parameters were previously used to investigate ion pairing in rigid SPC water.[7] The cross-interaction parameters are derived using the Lorentz−Berthelot combining rules[29] using the same approach as others.[17,30] All pure component interaction parameters are reported in Table 1.

Molecular Dynamics Simulations. Canonical (constant NVT) ensemble molecular dynamics simulations were conducted to determine the ion solvation properties with the flexible SPC water model. The metal ion and two chloride ions were added to a cubic 25.0 Å × 25.0 Å × 25.0 Å simulation cell, with 512 water molecules at a water density of 1.00 g/cm^3. The ion concentration in the simulation cell was 0.1 M. Equilibration periods of 0.05 ns in the microcanonical (constant NVE) ensemble were followed by 10 ns production runs in the NVT ensemble. Statistics of the production run were collected every 1 ps. A Nose−Hoover thermostat[31,32] with a relaxation time of 0.1 ps was used to maintain an average temperature of 300 K. Solvation properties (radial distribution functions and coordination numbers) of each ion were evaluated with the flexible SPC water model.

In addition, isothermal−isobaric (constant NPT) ensemble molecular dynamics simulations were conducted to investigate the ion pairing dependence on concentration. The MCl_2 salt simulations were conducted at concentrations ranging from 0.22 to 3.5 M in a cubic simulation cell with 1024 water molecules. The NPT ensemble was chosen for these calculations to allow for variations in system volume and density resulting from different ion concentrations. NPT simulations of 10.0 ns in length were performed, after short (0.05 ns) equilibration runs

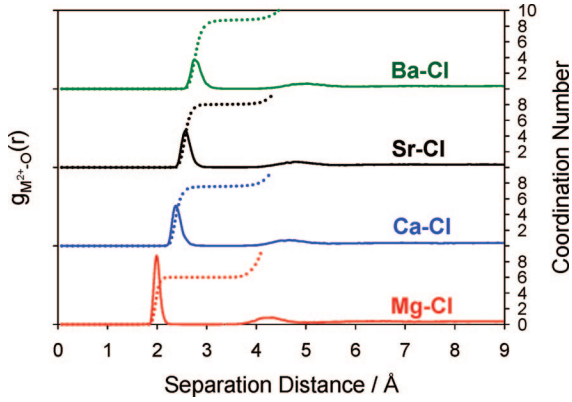

Figure 1. M^{2+}−H_2O radial distribution function and coordination number as a function of radial distance. The radial distribution functions are given by the solid lines and the coordination numbers are given by the dotted lines. For clarity, the radial distribution function curves for each metal are offset from each other by 35 arbitrary units on the *y*-axis. Each of these curves asymptotically converges to unity. The right-hand ordinate scale provides coordination numbers.

TABLE 3: The Aqueous Ion−Water M^{2+}-OH_2 Distances, Coordination Numbers, And Hydration Free Energies As Compared with Various Experimental Approaches (Observed)

			calculated		experiment	
ion	ionic radius (Å)	$\Delta G_{hyd}^{obs,a}$ (kcal/mol)	r_{max} (Å)	C.N	r_{max}^{obs} (Å)	C.N.^{obs}
Mg^{2+}	0.86	−455.5	1.98	6.0	2.00−2.15[b]	6
Ca^{2+}	1.26	−380.8	2.38	7.5	2.42−2.47[c,d,e,f,g]	7 − 8.1[c−g]
Sr^{2+}	1.40	−345.9	2.58	8.0	2.57−2.65[b,c,d,e,f,g,h,i]	6 − 10[b,h−m]
Ba^{2+}	1.56	−315.1	2.78	8.8	2.75[b]	9.5[b]
Cl^-	1.67	−75.8	3.23	7.3	3.24−3.25[e]	6[e,n]

[a] Friedman and Krishnan:[67] Free energies are all based on measured ionization potentials or electron affinities and are based on compilations. [b] Ohtaki and Radnai:[39] Compilation of EXAFS and X-ray diffraction data. [c] Smirnov.[68] [d] Fulton et al.[51] [e] Jalilehvand.[19] [f] Sandstrom.[69] [g] D'Angelo.[70] [h] Seward et al.[3] [i] O'Day et al.[71] [j] Parkman et al.[72] [k] Pfund et al.[73] [l] Persson et al.[74] [m] Palmer et al.[75] [n] Megyes et al.[53,54] The ionic radii are given as an indication of the relative size of each ion.

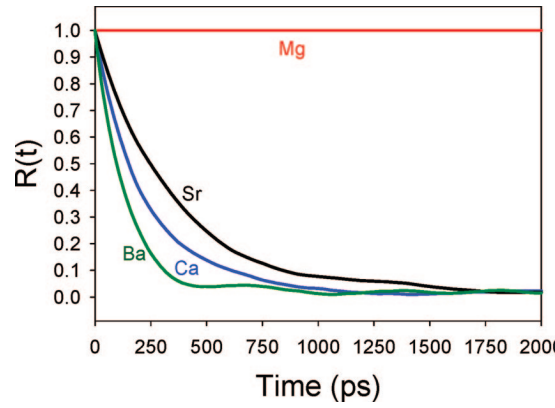

Figure 2. The residence time correlation function.

TABLE 4: The Water Residence Times in the First Hydration Shell

	residence time (sec)	
metal	calculated	experiment[42,45,48]
Mg^{2+}	$>1.0 \times 10^{-8}$	$6.7 \pm 0.2 \times 10^{-5}$
Ca^{2+}	4.91×10^{-11}	3.1×10^{-9}
Sr^{2+}	4.31×10^{-11}	2.5×10^{-9}
Ba^{2+}	1.46×10^{-11}	1.2×10^{-9}

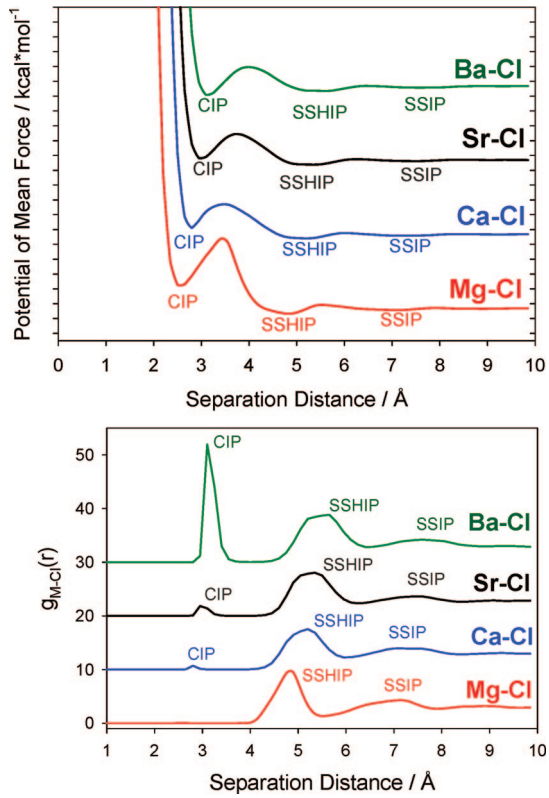

Figure 3. Radial dependence of the potential of mean force and pair-distribution function. For comparison, each alkaline earth metal−chloride ion pair (Mg−Cl, red; Ca−Cl, blue; Sr−Cl, black; Ba−Cl, green) are offset from one another by 10 kcal/mol (a) and 10 units (b).

in the NVE ensemble. The simulation cell lengths were allowed to expand or contract isotropically to maintain an average pressure of 1 atm at 300 K. The Nose−Hoover barostat and thermostat[31,33] relaxation times were 1.0 and 0.1 ps, respectively. For each MCl_2 NPT simulation, the number of ion pairs as well as the average cell lengths and system concentrations are reported in Table 2.

For all molecular dynamics simulations, the velocity Verlet integration algorithm was used to update positions every 1.0 fs. Full periodic boundary conditions were employed with an interaction cutoff of half the smallest simulation cell length. The long-range Coulombic interactions were evaluated using the Ewald summation method.[34] The Ewald precision value was set to 1×10^{-4} for all simulations. This value ultimately sets the number of *K*-space vectors, which are computed internally through the LAMMPS simulation software.[24,25]

Potential-of-Mean-Force Calculations. The free energy profile between the dissociated and associated ion pair states is mapped through potential-of-mean-force calculations to examine metal−chloride association in aqueous solution. In this approach, the ion pair is brought from infinite separation and gradually reduced to a separation distance *r*. The potential of mean force, $W_{M\text{-}Cl}(r)$, between the alkaline earth metal, M^{2+} and the chloride ion, Cl^- is obtained by integration of the mean force, $F(r)$, along the reaction coordinate pathway and given by the relation

$$\Delta W_{M-Cl}(r) = -\int_{r_0}^{r} F(r)\,dr \qquad (2)$$

To obtain the mean force, $F(r)$, the SHAKE algorithm[35] was used to constrain the ion pair separation at a distance *r*. The constant of integration, $W_{M\text{-}Cl}(r_0)$, at the reference distance, r_0, corresponds to the limiting continuum behavior at the largest ion pair separation distance and is approximated by the relation

$$W_{M-Cl}(r_0) \approx \frac{q_i q_j}{\varepsilon r_0} \qquad (3)$$

where q_i is the charge on ion *i* and ε is the dielectric constant of the solvent.[1] The dielectric constant for the SPC water is reported as 78.2,[36] and r_o was selected to be 10 Å. A detailed review of the potential of mean force is given elsewhere.[1,37]

A total of 61 canonical ensemble (NVT) molecular dynamics simulations were conducted for 0.5 ns at 300 K to obtain the free energy profiles of each respective metal−chloride pair. The simulated density of water in the cubic 24.9 Å × 24.9 Å × 24.9 Å simulation cell was 1.00 g/cm^3 (N = 512 water molecules, 1 M^{2+}, 2 Cl^-). The ion pair constrained distance was varied from 1.0 Å to 10.0 Å, with intermediate step sizes of 0.15 Å. Statistics on the mean force were collected every time step over a 0.5 ns simulation. Charge neutrality was maintained by allowing the additional chloride ion to move unconstrained throughout the simulation cell. Finally, the potential of mean force was obtained through numerical integration using Simpson's rule.[38]

3. Results and Discussion

3.1. Hydration Structure of Alkaline Earth Metal Cations. The hydration structural properties for each aqueous ion (Mg^{2+}, Ca^{2+}, Sr^{2+}, Ba^{2+}) are computed from canonical NVT ensemble molecular dynamics simulations. The average metal−oxygen distances and coordination numbers of 0.1 M solutions are determined from the radial distribution functions (RDF), which are shown in Figure 1 and provided in Table 3. The first peak maximum represents the average metal−oxygen distance and the first peak minimum is characteristic of the outer radius of the first solvation shell.

In general, for the alkaline earth metals, the M^{2+}-H_2O distance and coordination number increases as a function of cation size (Mg^{2+} < Ca^{2+} < Sr^{2+} < Ba^{2+}). The resulting peak maxima and coordination numbers are consistent with X-ray diffraction, neutron diffraction, and EXAFS experiments,[39] demonstrating that the flexible SPC water model in combination with the force field parameters for the alkaline earth metals adequately predict the geometry of the first hydration shell around each of the metals.

In addition to the structural information, the force field parameters were previously parametrized to the hydration free energies through the free energy pertubation method.[28] The hydration free energies measured from experiments are provided in Table 3. In general, the interaction strength between water and the metal cation increases as the ion radius decreases, indicating that it is more difficult to remove a water molecule from the Mg^{2+} hydration shell than from the Ba^{2+} hydration shell.

TABLE 5: Calculated Potential Energy Minima, Maxima, and Free Energy Barriers

	CIP min	SSHIP min	SSIP min	CIP|SSHIP max	CIP → SSHIP E_a	SSHIP → CIP E_a	SSHIP|SSIP max	SSHIP → SSIP E_a	SSIP → SSHIP E_a
$MgCl^+$	2.53	−1.34	−0.87	8.72	6.19	10.06	−0.16	1.18	0.71
$CaCl^+$	0.22	−1.20	−0.82	3.38	3.16	4.60	−0.49	0.71	0.33
$SrCl^+$	−0.36	−1.24	−0.77	2.87	3.23	4.12	−0.51	0.74	0.26
$BaCl^+$	−1.84	−1.30	−0.86	1.92	3.76	3.22	−0.62	0.67	0.23

3.2. Water Residence Times. The mean residence time of water molecules in the solvation shell is determined by the rate of exchange between these molecules and those in the bulk solution. It is calculated from the time correlation function[40,41] defined by

$$R(t) = \frac{1}{N_c}\sum_{i=1}^{N_c} \langle \theta_i(t)\, \theta_i(0) \rangle \quad (4)$$

where θ_i is the Heaviside unit step function and N_c is the number of water molecules in this shell. The residence time of water, τ, in the hydration shell can be calculated by integrating the residence time correlation function

$$\tau = \int_0^\infty R(t)\, dt \quad (5)$$

The time correlation functions are illustrated in Figure 2, and the computed residence times are reported in Table 4.

Interestingly, the time correlation function of Mg^{2+} does not decay over the 10 ns time scale of our molecular dynamics simulations. Examination of the snapshots over the duration of these 10 ns molecular dynamics simulations shows no exchange of water from the first hydration shell to the second hydration shell. In fact, experimentally measured residence times are measured to be on the order of microseconds,[42−44] indicating that water residence times of Mg^{2+} cannot be computed with traditional computational techniques. Water residence times for Ca^{2+}, Sr^{2+}, and Ba^{2+} deduced from ligand substitution experimental studies are 2 orders of magnitude shorter;[43−45] however, the computed residence times are consistent with other simulation studies.[17,46,47] Given the decrease in interaction strength (less negative hydration free energies) between the ion and water with increasing ion size, the residence times for water in the first hydration shell decrease. This trend is observed both in the simulated and experimentally derived water residence times.

3.3. Ion-Pair Free Energy Profiles. The free energy profiles and pair distribution functions for each MCl^+ complex at infinite dilution are shown in Figure 3. The pair distribution function, $g^\infty_{M-Cl}(r)$, between the alkaline earth metal M^{2+} and chloride ion Cl^- is related to the potential of mean force through the equation

$$W_{M-Cl}(r) = -k_B T \ln g^\infty_{M-Cl}(r) \quad (6)$$

where the superscript ∞ indicates infinite dilution, k_B is Boltzmann's constant and T is the temperature of the simulation.

Each of the free energy profiles exhibit three local minima that correspond to three different types of ion pairs: (1) a contact ion pair (CIP) where the metal cation and chloride anion are in direct contact with each other, (2) a solvent shared ion pair (SSHIP) where the cation and anion are separated by one water molecule, and (3) a solvent-separated ion pair (SSIP) where both the cation and anion retain one full hydration shell and the ions are separated by two water molecules.[48−50] The calculated values for the local minima for each type of ion pair as well as for the free energy barriers between each type of ion pair are reported in Table 5.

The formation of a CIP requires the removal of a water molecule from the first hydration shell of the metal to accommodate the associating anion. Figure 3A shows that the free energy barrier to remove a water molecule from the first hydration shell and form a CIP from an SSHIP decreases with increasing ion size from Mg^{2+} to Ba^{2+}. In addition, the stability of the CIP relative to the SSHIP increases as the ion radius increases (i.e., $Mg^{2+} < Ca^{2+} < Sr^{2+} < Ba^{2+}$).

The formation of a metal−chloride CIP is correlated to its hydration free energy (Table 3). As the metal-water binding strength decreases (less negative hydration free energies) from Mg^{2+} to Ba^{2+}, the activation barrier from SSHIP to CIP decreases. The activation energy barrier for Mg^{2+} (nearly 10 kcal/mol) is significantly higher than all other alkaline earth metals (<5 kcal/mol), indicating that a large amount of thermal energy is required to release a water molecule from the Mg^{2+} hydration shell and replace it with a chloride ion. In addition, the $MgCl^+$ CIP complex is thermodynamically less stable than the $MgCl^+$ SSHIP complex; the difference in free energy between the two local minima is approximately +4 kcal/mol (Figure 3A). The pair distribution function of Mg^{2+} in Figure 3B (eq 6) exhibits no maximum for the $MgCl^+$ CIP complex, indicating that this complex will not form at ambient conditions and low concentrations. Furthermore, the simulations show that the $MgCl^+$ SSHIP complex is preferred at equilibrium.

The $CaCl^+$ free-energy profile exhibits similar behavior to the $MgCl^+$ profile. However, the activation-energy barrier from SSHIP to CIP is much smaller (∼5 kcal/mol) than $MgCl^+$. Moreover, the difference in the local free-energy minima for the $CaCl^+$ SSHIP and CIP complexes is much smaller than for $MgCl^+$ (∼1 kcal/mol). A small peak for the CIP $CaCl^+$ complex is present in the pair distribution function (Figure 3B), along with a larger peak for the SSHIP complex, indicating that the SSHIP complexes are the predominant complexes in solution at equilibrium. This conclusion is consistent with other investigators who examined the formation of $CaCl^+$ complexes using the rigid SPC/E model and a different set of ion−water parameters.[5−7] It is also consistent with X-ray absorption fine structure (EXAFS) and pre-edge and near edge (XANES) spectra for 6 m $CaCl_2$ that yielded no evidence for the formation of significant numbers of $Ca^{2+}-Cl^-$ CIPs.[51] Instead, these spectroscopic studies as well as neutron diffraction isotope substitution (NDIS) data[52] provide evidence for the formation of $Ca^{2+}-OH_2-Cl^-$ SSHIPs. Evidence for both types of ion pairs was found at high concentrations using X-ray diffraction experiments.[53,54]

The activation energy barriers to form a CIP from an SSHIP for $SrCl^+$ and $BaCl^+$ are smaller than $CaCl^+$ (see Figure 3A). For $SrCl^+$, the free energy minima for both the CIP and SSHIP complexes are similar in magnitude. For $BaCl^+$, the minimum in free energy for the CIP is slightly lower than for the SSHIP, indicating that CIP formation is more favorable. In response to the weaker metal-water interactions and the shorter water residence times, the CIP complexes for Sr^{2+} and Ba^{2+} are more stable than for Mg^{2+} and Ca^{2+}. Because the potential of mean force calculations show that the stabilities of the CIP and SSHIP are similar for both $SrCl^+$ and $BaCl^+$, the calculated pair distribution functions indicate that both complexes are present at equilibrium (Figure 3B).

3.4. Metal Complexation Dependence on Concentration. The ion pairing dependence on the MCl_2 salt concentration is examined through NPT ensemble molecular dynamics simulations. In Figure 4, speciation diagrams for each metal are shown as a function of metal concentration. The metal complexes are described as CIP, SSHIP, or SSIP if a metal−chloride complex forms, and as free ions (FI) if the metal is not associated with an anion. These assignments are made according to the metal−chloride distance, where the maximum distance for a particular type of ion pair is equal to the separation distance corresponding to the minimum free energy configuration in the PMF profiles. In general, as the MCl_2 salt concentration is increased, the number of associated contact ion pairs increases.

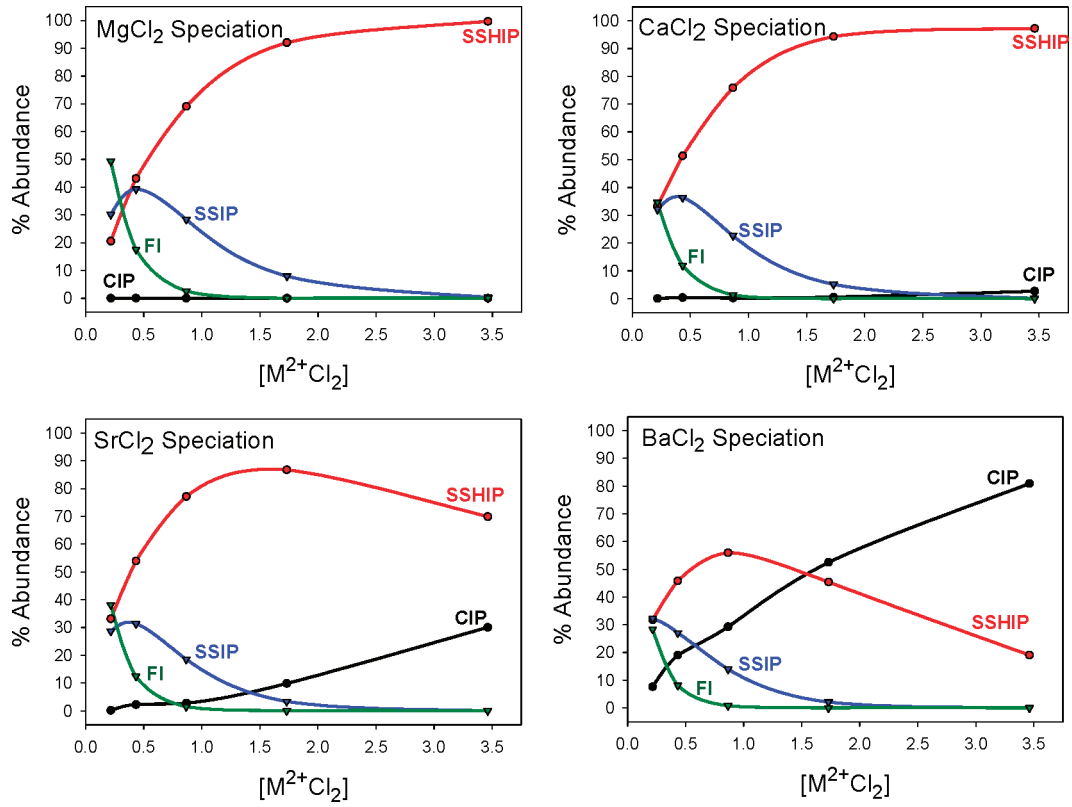

Figure 4. Speciation diagrams of each metal−chloride ion pair as a function of the average salt concentration computed through the NPT simulations. The CIP presence increases with increasing ionic radius.

The smaller metal ions (Mg^{2+} and Ca^{2+}) form essentially no contact ion pairs (CIP) over the range of concentrations investigated. However, the percentage of solvent shared ion pairs (SSHIP) increases as the molar concentration increases, suggesting that the SSHIP is thermodynamically favored. For Sr^{2+} and Ba^{2+}, the increase in CIP results in a decrease in SSHIP, suggesting that the equilibrium ratio of complexes shifts toward the CIP as the molar concentration increases. In each system, the number of SSIP and FI decreases rapidly to zero as the concentration increases.

Finally, it is worth noting that the results from the $MgCl_2$ system are highly dependent on the initial configuration. Initial configurations in which a chloride ion was located within the CIP radial distance of Mg^{2+} resulted in a CIP for the duration of the 10 ns molecular dynamics simulation. This suggests that the timescales of the molecular dynamics simulations (ns) are too short to overcome the activation energy barrier to go from a CIP to a SSHIP. This hypothesis is supported by the free energy profiles for the different metals in Figure 3A that show that the activation energy barrier from CIP to SSHIP is larger for Mg^{2+} than the other metals. In addition, the free energy profile for Mg^{2+} shows that the SSHIP is thermodynamically preferred over the CIP. Therefore, the ions are kinetically trapped in the CIP configuration, and more efficient sampling strategies would be needed to overcome these barriers. Additional simulations were conducted to ensure that the initial configuration did not include any biasing toward the CIP. For the $MgCl_2$ system, the initial configuration contained no CIPs (i.e., the initial separation distances between neighboring Mg and Cl ions were greater than the CIP/SSHIP activation barrier distance of 3.5 Å computed through the potential of mean force calculations). The resulting speciation scheme is given in Figure 4, where no CIPs are observed over the duration of the MD simulations. While the $MgCl_2$ system was affected by poor sampling, the remaining alkaline earth metal−chloride systems can easily overcome the free energy barriers between ion pair types to establish a true equilibrium.

3.5. Calculation of Ion-Pair Association Constants. The Eigen concept that ions sequentially form three types of ion pairs (SSIP, SSHIP, and CIP) is reinforced by the PMF approach and can be written as the following reaction series:

$$\underset{\text{free ions}}{M^{2+}(aq) + Cl^{-}(aq)} \overset{K_1}{\longleftrightarrow} \underset{\text{SSIP}}{[M^{2+}(OH_2)(OH_2)Cl^{-}]} \overset{K_2}{\longleftrightarrow} \underset{\text{SSHIP}}{[M^{2+}(OH_2)Cl^{-}]} \overset{K_3}{\longleftrightarrow} \underset{\text{CIP}}{[MCl^{+}]} \quad (7)$$

where M^{2+} and Cl^{-} represent the alkaline earth metal and chloride ions, respectively, and MCl^{+} represents the ion pair.[49,50] Traditional approaches to measuring ion-pairing in aqueous solution such as potentiometry with ion-selective electrodes or electrophoresis detect an overall association constant (K_a), which can be written as a composite of the equilibrium constants K_1, K_2, and K_3:[49,50]

$$K_a = K_1 + K_1K_2 + K_1K_2K_3 \quad (8)$$

The association constants for $MgCl^{+}$, $CaCl^{+}$, $SrCl^{+}$, and $BaCl^{+}$ determined by Majer and Stulik[55] by potentiometry with a chloride ion-selective electrode for 25 °C, 1 bar, and infinite dilution are reported in Table 6. In general, the experiments show that the stability of the ion pairs decreases with increasing cation radii.

Following the approach presented by Chialvo et al.,[56] the association constant at infinite dilution was computed from the expression:

$$K_a = 2\pi \int_0^{\text{SSIP|FI}} g^{\infty}_{M-Cl}(r)\, r^2\, dr \quad (9)$$

where $g^{\infty}_{M-Cl}(r)$ is the pair distribution function at infinite dilution between the alkaline earth metals M^{2+} and chloride ion Cl^-. The upper limit of integration "SSIP|FI" represents the minimum in $g^{\infty}_{M-Cl}(r)$ between the SSIP peak and the free ions. For validation purposes, these association constants were also calculated by combining eq 8 with expressions similar to eq 9 for K_1, K_2, and K_3. Both approaches led to the constants reported in column 3 of Table 6.

Alternatively, the association constant at infinite dilution can be obtained by extrapolation of the concentration-dependent stability constant, $K(C)$. The stability constants at four concentrations (0.22 M, 0.43 M, 0.86 M, and 1.73 M) used in the NPT MD simulations were computed through the expression

$$K(C) = \frac{[\text{SSIP} + \text{SSHIP} + \text{CIP}]}{[\text{FI}][\text{Cl}^-_{aq}]} = \frac{[\text{SSIP} + \text{SSHIP} + \text{CIP}]}{[\text{FI}][2M_T - (\text{SSIP} + \text{SSHIP} + \text{CIP})]} \quad (10)$$

where M_T is the total concentration of metal in solution and $2M_T$ is the total concentration of chloride in solution. For each system, a regression line was fit to the log $K(C)$ vs M_T to compute the association constant at infinite dilution (see Appendix A for more details). These association constants are reported in column 4 of Table 6 and are compared in the table to those calculated using eq 8 in combination with equations similar to eq 9 for K_1, K_2, and K_3. The two approaches, which should lead to identical association constants, differed by between 17 and 46%. This outcome suggests that much longer counting times are required to determine association constants from the NPT MD simulations.

The association constants, calculated using either eq 9 or eq 10, suggest that the stability of alkaline earth metal−chloride ion pairs increases with increasing cation radii. This trend is the opposite of that established from the experimental data of Majer and Stulik.[55] This discrepancy in MCl^+ stability as a function of ion size may be due to several different sources of uncertainty. Although the experimental data indicate decreasing association with increasing metal radius at 25 °C, this trend was not observed at 15 or 45 °C (see Table 7). The error bars on the association constants determined at 25 °C are large, such that the ranges of values defined by one standard deviation overlap for the formation of $MgCl^+$, $CaCl^+$, and $SrCl^+$, demonstrating the difficulty associated with deriving experimental association constants for weakly associating ion pairs. Uncertainties associated with the force field model are discussed below.

TABLE 6: Comparison of Experimental and Calculated Association Constants

	K_a (exptl)[a]	K_a (eq 9)	K_a (eq 10)
$MgCl^+$	0.77 ± 0.23	0.645	0.656
$CaCl^+$	0.68 ± 0.08	0.798	1.418
$SrCl^+$	0.54 ± 0.08	0.775	2.324
$BaCl^+$	0.34 ± 0.07	1.110	2.416

[a] Majer and Stulik (1982).[55]

TABLE 7: Experimental Association Constants at Different Temperatures (Major and Stulik[55])

		$MgCl^+$	$CaCl^+$	$SrCl^+$	$BaCl^+$
15 °C	K_{avg}	0.72	0.54	0.56	0.25
	range (±1 σ)	0.64−0.80	0.45−0.63	0.51−0.61	0.18−0.32
25 °C	K_{avg}	0.77	0.68	0.54	0.34
	range (±1 σ)	0.54−1.00	0.60−0.76	0.46−0.62	0.27−0.41
45 °C	K_{avg}	0.83	0.63	0.89	0.66
	range (±1 σ)	0.79−0.87	0.56−0.70	0.79−0.94	0.48−0.84

4. Conclusions

The force field parameter set used in this study successfully predicts many of the structural and hydration properties of the ions and, in addition, several of the trends expected in M^{2+}-Cl^- pairing. In general, for the alkaline earth metals, the calculated M^{2+}−H_2O distance and coordination number increase as a function of cation size ($Mg^{2+} < Ca^{2+} < Sr^{2+} < Ba^{2+}$) and are consistent with experimental measurements. These results demonstrate that the flexible SPC water model in combination with the force-field parameters for the alkaline earth metals adequately predict the geometry of the first hydration shell around each metal. Experimental residence times for water within the first hydration shell for the alkaline earth metal cations exhibit a trend of decreasing residence time with increasing ion radius. This trend is not entirely reproduced by the calculations, largely because the residence time for H_2O in the solvation shell for Ca^{2+} is slightly shorter than for H_2O in the solvation shell for Sr^{2+}. However, the dramatic difference between the residence time for water molecules in the Mg^{2+} solvation shell and in the other cation solvation shells is reproduced by the force-field parametrization. Consistent with other modeling studies, calculated residence times for Ca^{2+}, Sr^{2+}, and Ba^{2+} are roughly 3 orders of magnitude smaller than those determined experimentally.

For $MgCl^+$, $CaCl^+$, and $SrCl^+$, the activation energies associated with forming a CIP from a SSHIP are larger than those for forming a SSHIP from a CIP. The calculated activation energy barriers for converting from a SSHIP to SSIP, or vice versa, are much smaller than those involved in the CIP to SSHIP reactions. These results emphasize the impact of the metal hydration free energy in ion-pair formation.

The potential energy minima associated with the formation of CIPs for all four metals suggest that ion-pair stability increases with increasing cation size. This trend is reproduced by our calculated association constants. However, this trend is inconsistent with the experimentally derived association constants reported in the literature. There are numerous factors that may contribute to this inconsistency. First, the force field parameter set was not directly optimized for the M^{2+}−Cl^- interactions. Instead the cross-terms for the M^{2+}−Cl^- interactions were determined using the Lorentz−Berthelot combining rules.[29] Incorporating explicit cross-terms for the Lennard Jones interactions between M^{2+} and Cl^- into our model might improve the calculated trend in metal−chloride association.

One approach to investigating the performance of the M^{2+}−Cl^- interaction parameter set is to compare calculated M^{2+}−Cl^- distances with those determined experimentally. X-ray diffraction,[53] neutron diffraction,[52−54] XAFS,[54] and LAXS[54] techniques have all been used to investigate Ca^{2+}−Cl^- interactions. Experimentally derived distances between M^{2+} and Cl^- at 25 °C, for concentrations similar to those in our simulations, are between 2.73 and 2.75 Å for the CIP and between 4.85 and 5.01 Å for the SSHIP. These distances are both smaller than the distances found in our simulations (i.e., 2.80 and 5.2 Å for the CIP and SSHIP, respectively; see Figure 3). The distance between Sr^{2+}−Cl^- for a CIP was found to be 2.86 Å using EXAFS,[16] while our calculations gave a distance of 2.95 Å. The longer calculated distances are to be expected given that the ions are represented by hard, single point charge spheres in our force-field model.

The use of a polarizable water model in combination with a set of polarizable ion−water intermolecular potential models may reduce the distance between ions in the ion pairs. The need to use polarizable potential models to describe the solvation of anions like Cl^- has been discussed in the literature. Using a set of polarizable potential models, Dang et al.[10] calculated that the first solvation shell around Cl^- is asymmetric, with four water molecules hydrogen-bonded together on one side of the anion. Smith and Dang[8] concluded that the use of a polarizable water model did not result in major differences in calculated Na^+Cl^- association, but suggested that polarizability would be essential to describing divalent-ion hydration. Major differences in calculated ion distributions at the air−water interface arise from using nonpolarizable and polarizable potential models.[57−61] The distribution of anions observed at the air−water interface can be more accurately simulated when the polarizability of the anions is considered. For Cl^-, this means that more of the anions are exposed and available for reaction at the air−water interface.[59]

Finally, the specific combination of ion−water potentials used in our simulations may have given rise to the inverse of the observed trend in $M^{2+}-Cl^-$ association. Computational and spectroscopic approaches to investigating ion hydration have both been advancing rapidly, sometimes together. Guardia et al.[21] calculated the thermodynamic and dynamic properties of Ca^{2+} in solution using three different Ca^{2+}-water potentials and concluded that there was not sufficient experimental data to select the best potential.[62] Jalilehvand et al.[62] tried three different Ca^{2+}−water potentials and selected the one that provided simulation results consistent with experimental data from EXAFS and large-angle X-ray scattering (LAXS). For our research, we chose to use the $M^{2+}-H_2O$ potentials of Åqvist[28] because they were derived systematically by one research group using one technique. However, the $Cl^-−H_2O$ potential of Dang et al.[7] was not developed using the same method. Another $Cl^-−H_2O$ potential combined with Åqvist's alkaline earth metal−water potentials might reproduce the experimental trend in alkaline earth metal−chloride association. Given the new spectroscopic and diffraction data that have been collected since Åqvist[28] developed his alkaline-earth metal−water potentials, a review of these force field parameters might be timely.

In summary, there are numerous possible approaches that might improve the calculated association constants. Additional data, such as the dielectric relaxation spectral data collected for other aqueous ion pairs,[63−66] that provides information on the ratios of CIPs, SSHIPs, and SSIPs in solution, would greatly enhance our ability to select the best approach to improve force-field models such that bulk thermodynamic trends in aqueous speciation can be calculated effectively.

Acknowledgment. We would like to acknowledge constructive discussions with R. T. Cygan and J. L. Krumhansl. Early reviews by and discussion with J. A. Greathouse, G. Hefter, and J. R. Rustad greatly improved this manuscript. H. Finley-Jones and J. Durkin contributed by performing some of the molecular dynamics simulations and maintaining our computer clusters. This research was supported by the U.S. Department of Energy, Office of Basic Energy Sciences, Division of Chemical Sciences, Geosciences, and Biosciences. Sandia National Laboratories is a multiprogram laboratory operated by the Sandia Corporation, a Lockheed Martin Company for the United States Department of Energy's National Nuclear Security Administration under Contract DE-AC04-94AL85000.

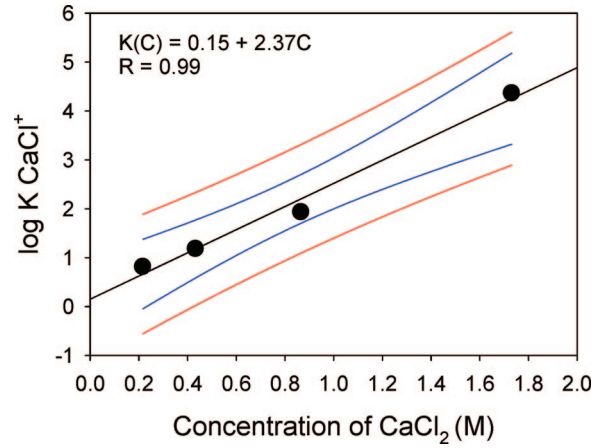

Figure 5. Plot of $K(C)$ determined from average ion-pair distributions found in NPT simulations at four different MCl_2 concentrations. The association constant for MCl^+ at infinite dilution is determined by linear regression through a concentration of zero.

Appendix

Derivation of Equation 10 for the Association Constant K_a

The Eigen concept that ions sequentially form three types of ion pairs (SSIP, SSHIP, and CIP) is reinforced by the PMF approach and can be written as the following reaction series:

$$\underset{\text{free ions}}{M^{2+}(aq) + Cl^-(aq)} \overset{K_1}{\longleftrightarrow} \underset{\text{SSIP}}{[M^{2+}(OH_2)(OH_2)Cl^-]} \overset{K_2}{\longleftrightarrow} \underset{\text{SSHIP}}{[M^{2+}(OH_2)Cl^-]} \overset{K_3}{\longleftrightarrow} \underset{\text{CIP}}{[MCl^+]} \quad (1a)$$

where M^{2+} and Cl^- represent the alkaline earth metal and chloride ions, respectively, and MCl^+ represents the ion pair. Traditional approaches to measuring ion-pairing in aqueous solution such as potentiometry with ion-selective electrodes or electrophoresis detect an overall association constant (K_a), which can be written as a composite of the equilibrium constants K_1, K_2, and K_3:

$$K_a(T,p) = K_1 + K_1K_2 + K_1K_2K_3 \quad (2a)$$

The equilibrium association constant for MCl^+ is

$$K_a(T,p) = \frac{a_{MCl^+}}{a_{M^{2+}}a_{Cl^-}} = \frac{[MCl^+]\gamma_{MCl^+}}{[M^{2+}][Cl^-]\gamma_{M^{2+}}\gamma_{Cl^-}} \quad (3a)$$

where a_i is the activity of the species i; $MCl^+ \equiv$ SSIP + SSHIP + CIP; γ_{MCl^+}, $\gamma_{M^{2+}}$, γ_{Cl^-} are the activity coefficients for MCl^+ and the free ions M^{2+} and Cl^- in solution; and [...] denotes a molar concentration. The total concentration of M^{2+} in solution is $M_T = [M^{2+}] + [MCl^+]$. At infinite dilution, the activity coefficients approach unity and can be neglected. Assuming that the activity coefficients can be ignored at any concentration, C,

$$K(C) = \frac{[MCl^+]}{[M^{2+}][Cl^-]} = \frac{[\text{SSIP} + \text{SSHIP} + \text{CIP}]}{[\text{FI}][2M_T - (\text{SSIP} + \text{SSHIP} + \text{CIP})]} \quad (4a)$$

where FI is the number of free M^{2+} in aqueous solution, and $2M_T$ − (SSIP + SSHIP + CIP) is the number of free Cl^- ions. Note that mass balance requires that there are two chloride ions in solution for each metal ion (i.e., MCl_2). Using the ion pair

distribution provided in Figure 4, $K(C)$ for four concentrations were calculated using eq 4a. The data for the highest concentration available was ignored because the free metal ion concentrations (i.e., the denominator of eq 4a) in the simulations were zero. For each M^{2+}, the four $K(C)$ were plotted against C. Using linear regression, the best fit line through a solution concentration of zero was determined. In this way we obtained equilibrium constants at infinite dilution to compare to the constants determined using the potential of mean force calculations (see Figure 5).

References and Notes

(1) Chialvo, A. A.; Cummings, P. T.; Cochran, H. D.; Simonson, J. M.; Mesmer, R. E. *J. Chem. Phys.* **1995**, *103*, 9379.

(2) Chialvo, A. A.; Cummings, P. T.; Simonson, J. M.; Mesmer, R. E. *J. Mol. Liq.* **1997**, *73–74*, 261.

(3) Chialvo, A. A.; Cummings, P. T.; Simonson, J. M.; Mesmer, R. E. *J. Chem. Phys.* **1996**, *105*, 9248.

(4) Chialvo, A. A.; Cummings, P. T.; Simonson, J. M.; Mesmer, R. E. *J. Chem. Phys.* **1999**, *110*, 1064.

(5) Chialvo, A. A.; Simonson, J. M. *J. Chem. Phys.* **2003**, *118*, 7921.

(6) Dang, L. X. *J. Chem. Phys.* **1992**, *97*, 1919.

(7) Dang, L. X.; Rice, J. E.; Kollman, P. A. *J. Chem. Phys.* **1990**, *93*, 7528.

(8) Smith, D. E.; Dang, L. X. *J. Chem. Phys.* **1994**, *100*, 3757.

(9) Sherman, D. M.; Collings, M. D. *Geochem. Trans.* **2002**, *3*, 102.

(10) Dang, L. X.; Rice, J. E.; Caldwell, J.; Kollman, P. A. *J. Am. Chem. Soc.* **1991**, *113*, 2481.

(11) Guardia, E.; Rev, R.; Padro, J. A. *Chem. Phys.* **1991**, *155*, 187.

(12) Rey, R.; Guardia, E. *J. Phys. Chem.* **1992**, *96*, 4712.

(13) Chialvo, A. A.; Simonson, J. M. *J. Chem. Phys.* **2003**, *119*, 8052.

(14) Smith, D. E.; Dang, L. X. *Chem. Phys. Lett.* **1994**, *230*, 209.

(15) Dang, L. X.; Smith, D. E. *J. Chem. Phys.* **1995**, *102*, 3483.

(16) Seward, T. M.; Henderson, C. M. B.; Charnock, J. M.; Driesner, T. *Geochim. Cosmochim. Acta* **1999**, *63*, 2409.

(17) Zhu, Y.; Lu, X.; Ding, H.; Wang, Y. *Mol. Simul.* **2003**, *29*, 767.

(18) Dang, L. X.; Schenter, G. K.; Fulton, J. L. *J. Phys. Chem. B* **2003**, *107*, 14119.

(19) Jalilehvand, F.; Spangberg, D.; Lindqvist-Reis, P.; Hermansson, K.; Persson, I.; Sandstrom, M. *J. Am. Chem. Soc.* **2001**, *123*, 431.

(20) Spangberg, D.; Hermansson, K.; Lindqvist-Reis, P.; Jalilehvand, F.; Sandstrom, M. *J. Phys. Chem. B* **2000**, *104*, 10467.

(21) Guardia, E.; Sese, G.; Padro, J. A.; Kalko, S. G. *J. Solution Chem.* **1999**, *28*, 1113.

(22) Guardia, E.; Robinson, A.; Padro, J. A. *J. Chem. Phys.* **1993**, *99*, 4229.

(23) Guardia, E.; Padro, J. A. *J. Chem. Phys.* **1995**, *102*, 3485.

(24) Plimpton, S. J. *J. Comput. Phys.* **1995**, *117*, 1.

(25) Plimpton, S. J.; Pollock, R.; Stevens, M. "Particle-Mesh Ewald and rRESPA for parallel molecular dynamics simulations"; 8th SIAM Conference on Parallel Processing for Scientific Computing, Minneapolis, MN, 1997.

(26) Berendsen, H. J. C.; Postma, J. P. M.; vanGunsteren, W. F.; Hermans, J. Interaction models for water in relation to protein hydration. In *Intermolecular Forces*; Pullman, B., Ed.; D. Reidel, 1981; pp 331.

(27) Teleman, O.; Jonsson, B.; Engstrom, S. *Mol. Phys.* **1987**, *60*, 193.

(28) Aqvist, J. *J. Phys. Chem.* **1990**, *94*, 8021.

(29) Allen, M. P.; Tildesley, D. J. *Computer Simulation of Liquids*; Clarendon Press: Oxford, 1987.

(30) Gavryushov, S.; Linse, P. *J. Phys. Chem. B* **2006**, *110*, 10878.

(31) Melchionna, S.; Ciccotti, G.; Holian, B. L. *Mol. Phys.* **1993**, *78*, 533.

(32) Hoover, W. G. *Phys. Rev. A* **1985**, *31*, 1695.

(33) Hoover, W. G. *Phys. Rev. A* **1986**, *34*, 2499.

(34) Ewald, P. *Ann. Phys.* **1921**, *64*, 253.

(35) Ryckaert, T. P.; Ciccotti, G.; Berendsen, H. J. C. *J. Comput. Phys.* **1977**, *23*, 327.

(36) Mizan, T. I.; Savage, P. E.; Ziff, R. M. *J. Phys. Chem.* **1994**, *98*, 13067.

(37) Trzesniak, D.; Kunz, A. P. E.; van Gunsteren, W. F. *Chem Phys Chem* **2007**, *8*, 162.

(38) Press, W. H.; Teukolsky, S. A; Vetterling, W. T. ; Flannery, B. P. *Numerical Recipes: The Art of Scientific Computing*; Cambridge University Press: Cambridge, 1986.

(39) Ohtaki, H.; Radnai, T. *Chem. Rev.* **1993**, *93*, 1157.

(40) Impey, R. W.; Madden, P. A.; McDonald, I. R. *J. Phys. Chem.* **1983**, *87*, 5071.

(41) Koneshan, S.; Rasaiah, J. C.; Lynden-Bell, R. M.; Lee, S. H. *J. Phys. Chem. B* **1998**, *102*, 4193.

(42) Bleuzen, A.; Pittet, P. A.; Helm, L.; Merbach, A. E. *Magn. Reson. Chem.* **1997**, *35*, 765.

(43) Helm, L.; Merbach, A. E. *Chem. Rev.* **2005**, *105*, 1923.

(44) Burgess, M. A. *Metal Ions in Solution*; Ellis Horwood: Chichester, England, 1978.

(45) Helm, L.; Merbach, A. E. *Coord. Chem. Rev.* **1999**, *187*, 151.

(46) Koneshan, S.; Rasaiah, J. C.; Lynden-Bell, R. M.; Lee, S. H. *J. Phys. Chem. B* **1998**, *102*, 4193.

(47) Kerisit, S.; Parker, S. C. *J. Am. Chem. Soc.* **2004**, *126*, 10152.

(48) Marcus, Y. *Ion Solvation*; John Wiley & Sons: London, 1985.

(49) Marcus, Y.; Hefter, G. *Chem. Rev.* **2006**, *106*, 4585.

(50) Hefter, G. *Pure Appl. Chem.* **2006**, *78*, 1571.

(51) Fulton, J. L.; Heald, S. M.; Badyal, Y. S.; Simonson, J. M. *J. Phys. Chem. A* **2003**, *107*, 4688.

(52) Badyal, Y.; Barnes, A. C.; Cuello, G. J.; Simonson, J. M. *J. Phys. Chem. A* **2004**, *108*, 11819.

(53) Megyes, T.; Grosz, T.; Radnai, T.; Bako, I.; Palinkas, G. *J. Phys. Chem. A* **2004**, *108*, 7261.

(54) Megyes, T.; Bako, I.; Balint, S.; Grosz, T.; Radnai, T. *J. Mol. Liq.* **2006**, *129*, 63.

(55) Majer, V.; Stulik, K. *Anal. Data* **1982**, *29*, 145.

(56) Chialvo, A. A.; Cummings, P. T.; Cochran, H. D.; Simonson, J. M.; Mesmer, R. E. *J. Chem. Phys.* **1995**, *103*, 9379.

(57) Dang, L. X.; Chang, T.-M. *J. Phys. Chem. B* **2002**, *106*, 235.

(58) Dang, L. X. *J. Phys. Chem. B* **2002**, *106*, 10388.

(59) Knipping, E. M.; Lakin, M. J.; Foster, K. L.; Jungwirth, P.; Tobias, D. J.; Gerber, R. B.; Dabdub, D.; Finlayson-Pitts, B. J. *Science* **2000**, 301–306.

(60) Jungwirth, P.; Tobias, D. J. *J. Phys. Chem. A* **2002**, *106*, 379.

(61) Jungwirth, P.; Tobias, D. J. *J. Phys. Chem. B* **2002**, *106*, 6361.

(62) Jalilehvand, F.; Spangberg, D.; Lindqvist-Reis, P.; Hermansson, K.; Persson, I.; Sandstrom, M. *J. Am. Chem. Soc.* **2001**, *123*, 431.

(63) Wachter, W.; Kunz, W.; Buchner, R.; Hefter, G. *J. Phys. Chem. A* **2005**, *109*, 8675.

(64) Wahab, A.; Mahiuddin, S.; Hefter, G.; Kunz, W.; Minofar, B.; Jungwirth, P. *J. Phys. Chem. B* **2005**, *109*, 24108.

(65) Chen, T.; Hefter, G.; Buchner, R. *J. Solution Chem.* **2005**, *34*, 1045.

(66) Buchner, R.; Chen, T.; Hefter, G. *J. Phys. Chem. B* **2004**, *108*, 2365.

(67) Friedman, H. L.; Krishnan, C. V. Thermodynamics of Ionic Hydration. In *Water: A Comprehensive Treaty*; Frank, F., Ed.; Plenum Press: New York, 1973; Vol. 3; pp 472.

(68) Smirnov, P.; Yamagami, M.; Wakita, H.; Yamaguchi, T. *J. Mol. Liq.* **1997**, *73−4*, 305.

(69) Sandstrom, M.; Persson, I.; Jalilehvand, F.; Lindquist-Reis, P.; Spangberg, D.; Hermansson, K. *J. Synchrotron Radiat.* **2001**, *8*, 657.

(70) D'Angelo, P.; Petit, P. E.; Pavel, N. V. *J. Phys. Chem. B* **2004**, *108*, 11857.

(71) O'Day, P. A.; Newville, M.; Neuhoff, P. S.; Sahai, N.; Carroll, S. A. *J. Colloid Interface Sci.* **2000**, *222*, 184.

(72) Parkman, R. H.; Charnock, J. M.; Livens, F. R.; Vaughan, D. J. *Geochim. Cosmochim. Acta* **1998**, *62*, 1481.

(73) Pfund, D. M.; Darab, J. G.; Fulton, J. L.; Ma, Y. J. *J. Phys. Chem.* **1994**, *98*, 13102.

(74) Persson, I.; Sandstrom, M.; Yokoyama, H.; Chaudhry, M. *Z. Naturforsch. A* **1995**, *50*, 21.

(75) Palmer, B. J.; Pfund, D. M.; Fulton, J. L. *J. Phys. Chem.* **1996**, *100*, 13393.

JP802771W